Simple Protocol for Generating TiO_2 Nanofibers in Organic Media

Ruohong Sui, Venkataraman Thangadurai, and Curtis P. Berlinguette*

Department of Chemistry and The Institute for Sustainable Energy, Environment & Economy, University of Calgary, 2500 University Drive N.W., Calgary, Alberta, Canada T2N-1N4

Received July 30, 2008

Titania nanofibers in high yields can be accessed by treating titanium isopropoxide ($Ti(O^iPr)_4$) with acetic acid (AcOH) in heptanes when $R \geq 4.2$, where $R =$ mol of AcOH/mol of $Ti(O^iPr)_4$. Electron microscopic (SEM and TEM) images of the samples confirmed that high-aspect-ratio nanofibers with diameters in the 10−20 nm range are produced under these conditions, whereas agglomerated spherical nanoparticles are produced at $R \leq 3.8$. Powder X-ray diffraction and UV-vis data confirm the anatase crystalline phase after calcination at 400 °C, with the progressive formation of the rutile phase upon heating to higher temperatures. N_2 physisorption analyses showed the calcined fibers prepared at $R = 5.5$ have surface areas of 95 m^2/g. The self-assembly pathway leading to the nanofibers was delineated by in situ attenuated total reflection Fourier transform infrared (ATR-FTIR) spectroscopy in tandem with electrospray ionization mass spectrometry (ESI-MS). It was found that the hexanuclear building block, $Ti_6O_6(OAc)_6(O^iPr)_6$ (**TAC1**), is formed during the initial stages of the reactions, and that the axially ligated isopropoxide ligands of this complex are subsequently hydrolyzed to facilitate the one-dimensional condensation of the macromolecules at $R \geq 4.2$. Incomplete hydrolysis at lower acid ratios impedes this axial growth, resulting in spherical nanoparticles.

Introduction

Titanium dioxide (TiO_2) is a cheap and environmentally benign material that has found utility in a vast range of applications spanning photocatalysis,[1−5] photovoltaics,[6,7] sensing,[8,9] consumer products,[10,11] and others.[12,13] Consequently, a host of techniques have been documented describing the synthesis of TiO_2 materials that adopt a variety of shapes and sizes.[14] Of the architectures that have been established, one-dimensional (1D) TiO_2 structures on the nanoscale size regime are particularly attractive because of the unique chemical reactivity and photophysical behavior that arises when the morphology is restricted to a single direction.[15] While procedures for specifically accessing fibers, wires, and tubes are not as widespread compared to those for other geometries, a variety of methodologies have nonetheless emerged over the past decade; namely, hydrothermal,[16−18] electrospinning,[19,20] templating,[21−24] chemical vapor deposition (CVD),[25] high-temperature reformation of rutile,[26] titanium oxidation,[27] and sol−gel processes.[28,29] Although many of these approaches offer an impressive level of control and reproducibility for fabricating 1D TiO_2 nanostructures, the moderate reaction conditions characteristic of sol−gel chemistry stands out as one of the more attractive routes for large-scale commercial applications.[30] This procedure also provides the added benefit of accessing meso- and macroporous materials characterized by high surface areas, a prerequisite for many of the targeted applications.[31]

---

* Corresponding author. E-mail: cberling@ucalgary.ca.

(1) Fujishima, A.; Honda, K. *Nature* **1972**, *238*, 37–8.
(2) Bartl, M. H.; Boettcher, S. W.; Frindell, K. L.; Stucky, G. D. *Acc. Chem. Res.* **2005**, *38*, 263–271.
(3) Linsebigler, A. L.; Lu, G.; Yates, J. T. *Chem. Rev* **1995**, *95*, 735–58.
(4) Wold, A. *Chem. Mater.* **1993**, *5*, 280–3.
(5) Fujishima, A.; Rao, T. N.; Tryk, D. A. *J. Photochem. Photobiol. C: Photochem. Rev.* **2000**, *1*, 1–21.
(6) Gratzel, M. *Inorg. Chem.* **2005**, *44*, 6841–6851.
(7) Bisquert, J.; Cahen, D.; Hodes, G.; Ruhle, S.; Zaban, A. *J. Phys. Chem. B* **2004**, *108*, 8106–8118.
(8) Carotta, M. C.; Giberti, A.; Guidi, V.; Malagu, C.; Vendemiati, B.; Martinelli, G. *Mater. Res. Soc. Symp. Proc.* **2005**, *828*, 173–184.
(9) Akbar, S.; Yoo, S. *Chem. Sens.* **2004**, *20*, 30–31.
(10) Pfaff, G.; Reynders, P. *Chem. Rev.* **1999**, *99*, 1963–1982.
(11) Braun, J. H.; Baidins, A.; Marganski, R. E. *Prog. Org. Coat.* **1992**, *20*, 105–38.
(12) Wang, R.; Hashimoto, K.; Fujishima, A.; Chikuni, M.; Kojima, E.; Kitamura, A.; Shimohigoshi, M.; Watanabe, T. *Nature* **1997**, *388*, 431–432.
(13) Klemm, C.; Otto, S.; Wolf, C.; Haseloff, R. F.; Beyermann, M.; Krause, E. *J. Mass Spectrom.* **2006**, *41*, 1623–1632.
(14) Chen, X.; Mao, S. S. *Chem. Rev.* **2007**, *107*, 2891–2959.
(15) Kuchibhatla, S.; Karakoti, A. S.; Bera, D.; Seal, S. *Prog. Mater Sci.* **2007**, *52*, 699–913.
(16) Kolen'ko, Y. V.; Kovnir, K. A.; Gavrilov, A. I.; Garshev, A. V.; Frantti, J.; Lebedev, O. I.; Churagulov, B. R.; VanTendeloo, G.; Yoshimura, M. *J. Phys. Chem. B* **2006**, *110*, 4030–4038.
(17) Feng, X.; Zhai, J.; Jiang, L. *Angew. Chem.* **2005**, *117*, 5245–5248.
(18) Tahir, M. N.; Theato, P.; Oberle, P.; Melnyk, G.; Faiss, S.; Kolb, U.; Janshoff, A.; Stepputat, M.; Tremel, W. *Langmuir* **2006**, *22*, 5209–5212.
(19) Li, D.; Xia, Y. *Nano Lett.* **2003**, *3*, 555–560.
(20) Kim, I. D.; Rothschild, A.; Lee, B. H.; Kim, D. Y.; Jo, S. M.; Tuller, H. L. *Nano Lett.* **2006**, *6*, 2009–2013.
(21) Mor, G. K.; Shankar, K.; Paulose, M.; Varghese, O. K.; Grimes, C. A. *Nano Lett.* **2006**, *6*, 215–218.
(22) Miao, Z.; Xu, D.; Ouyang, J.; Guo, G.; Zhao, X.; Tang, Y. *Nano Lett.* **2002**, *2*, 717–720.
(23) Xiong, C.; Balkus, K. J. *Chem. Mater.* **2005**, *17*, 5136–5140.
(24) Weng, C. C.; Hsu, K. F.; Wei, K. H. *Chem. Mater.* **2004**, *16*, 4080–4086.
(25) Wu, J. J.; Yu, C. C. *J. Phys. Chem. B* **2004**, *108*, 3377–3379.
(26) Yoo, S.; Dregia, S. A.; Akbar, S. A.; Rick, H.; Sandhage, K. H. *MRS Bull.* **2006**, *21*, 1822–1829.
(27) Wu, J.-M.; Qi, B. *J. Am. Chem. Soc.* **2006**, *90*, 657–660.
(28) Boettcher, S. W.; Fan, J.; Tsung, C. K.; Shi, Q.; Stucky, G. D. *Acc. Chem. Res.* **2007**, *40*, 784–792.
(29) Schubert, U. *Acc. Chem. Res.* **2007**, *40*, 730–737.
(30) Brinker, C. J.; Scherer, G. W. *Sol−Gel Science: The Physics and Chemistry of Sol-Gel Processing*; Academic Press: New York, 1990.

10.1021/cm802091c CCC: $40.75

The sol−gel technique relies on the formation of a colloidal suspension, or sol, formed through the hydrolysis and polycondensation of molecular precursors, with subsequent polycondensation steps and concomitant solvent loss facilitating the formation of a well-defined solid network.[28,30,32] This versatile method has provided a convenient avenue for accessing a range of TiO_2 materials under moderate reaction conditions. Although a variety of molecular precursors and solvent media can be employed, a commonly used protocol is the controlled hydrolysis of titanium(IV) alkoxides. The subsequent condensation of the molecular fragments is dictated by a variety of reaction parameters, including the amount of water present and the choice surfactant.[28]

One of the initial reports of TiO_2 fibers produced by sol−gel chemistry relied on an organogelator and titanium isopropoxide ($Ti(O^iPr)_4$) to generate structures with diameters in excess of 1 μm.[33] Subsequent efforts have focused on reducing the diameter of the fibers to submicrometer scales to further increase the surface area to enhance the reactivity of the material.[34−43] Unfortunately, this goal is often accomplished largely by using expensive and/or complicated procedures that are not amenable to scale-up. Although aqueous sol−gel chemistry involving less exotic reagents (e.g., $Ti(OR)_4$, $TiCl_4$) yields various morphologies of TiO_2 architectures,[37,40,44] the interaction of water with the metal precursors readily forms a precipitate rendering little control over the structure of the final product. Thus, methods that afford greater control over the rate of the reaction are desired to help foster the growth of the desired nanostructures.

One approach circumvents aqueous media altogether by treating oleic acid with titanium alkoxide in anhydrous organic solvents to afford TiO_2 nanofibers with diameters as low as 2−4 nm.[43] Another key example is the synthesis of fibrous TiO_2 aerogels prepared by mixing titanium alkoxide with acetic acid (AcOH) in supercritical CO_2.[39] Despite providing access to fibers with diameters spanning the 10−100 nm range, the high pressures required to maintain the supercritical medium are not ideal for commercialization.

Building on these studies, we have established a low-temperature, ambient pressure method for synthesizing TiO_2 nanofibers characterized by high aspect ratios by treating $Ti(O^iPr)_4$ with AcOH in organic media. While similar reaction conditions are known to give rise to other TiO_2 morphologies,[45−48] we demonstrate that a nonpolar solvent such as heptanes serves as a suitable medium for producing nanofibers in high yields. The specific morphology of these structures is found to be inherently sensitive to the molar ratio of AcOH to the metal precursor, R (where R = mol AcOH/mol $Ti(O^iPr)_4$). We detail herein the facile synthetic conditions that give rise to these TiO_2 nanoscale architectures, along with an extensive examination of how R regulates the morphology of the final product.

Experimental Section

Materials. The starting materials $Ti(O^iPr)_4$ (97%) and AcOH (99.7%) were purchased from Alfa Aesar, and heptanes (99%) were purchased from Sigma Aldrich. All reagents were used as received.

Synthesis of TiO_2 Xerogels. Reactions were performed in a 50 mL round-bottom flask attached to a condenser, which was capped by a filter frit containing a layer of $MgSO_4$ to minimize exposure to moisture. The dried flask was heated in an oil bath to a temperature of 60 °C. The flask was then charged with 4.00 mL of heptanes (27.0 mmol), 2.02−4.74 mL of AcOH (35.2−82.5 mmol), followed by 3.37 mL of $Ti(O^iPr)_4$ (11.0 mmol). The homogeneous and light amber reaction mixture was maintained at a constant temperature of 60 °C with continuous stirring. The clear solution was converted to a white cloudy mixture within hours (t = 8, 5, and 2 h at R = 3.5, 5.5, and 7.5, respectively) followed by the formation of a gel; gelation times ranged from 7 h (R = 7.5) to ca. 10 days (R = 3.5). Each gel was aged for 5 days at 60 °C to promote further condensation, then dried in a vacuum oven (66.7 KPa) at 80 °C for 12 h. This was followed by a 2 h calcination at 400, 500, or 600 °C; each sample was brought to the respective temperature at a ramp rate of 5 °C/min. Following a 2 h holding time, the samples were cooled to room temperature at 5 °C/min. In a typical experiment, 0.86 g of TiO_2 xerogel was obtained after calcination corresponding to nearly quantitative yields based on the Ti starting material.

Physical Methods. Fourier transform infrared (FTIR) studies on solid samples were carried out on a Varian 7000 FTIR at a resolution of 4 cm^{-1}. Electronic spectroscopic data were collected on a Cary 5000 UV-vis Spectrophotometer (Varian) using a diffusive reflectance accessory. Sample preparation for UV analysis involved grinding the xerogels into a powder with a mortar and pestle, dispersing them in methanol, coating them onto a glass substrate, and then treating them at 80 °C for 8 h. X-ray diffraction (XRD) was performed using a Discovery D8 (Bruker-AXS) diffractometer employing Cu Kα radiation at 40 kV and 40 mA for the crystalline analysis. The Brunauer−Emmett−Teller (BET) surface area and pore size were obtained using an Autosorb (Quantachrome Instruments) at T = 77 K. Prior to N_2 physisorption data collection, the samples were degassed at 200 °C under vacuum at 6 μm Hg. Scanning electron microscopy (SEM) micrographs were recorded using a LEO 1530 at 2 kV with gold coating.

---

(31) Yang, P.; Zhao, D.; Margolese, D. I.; Chmelka, B. F.; Stucky, G. D. *Nature* **1998**, *396*, 152–155.

(32) Mackenzie, J. D.; Bescher, E. P. *Acc. Chem. Res.* **2007**, *40*, 810–818.

(33) Kobayashi, S.; Hanabusa, K.; Suzuki, M.; Kimura, M.; Shirai, H. *Chem. Lett.* **1999**, *10*, 1077–1078.

(34) Guo, C.-W.; Cao, Y.; Dai, W.-L.; Fan, K.-N.; Deng, J.-F. *Chem. Lett.* **2002**, *31*, 588–589.

(35) Miao, L.; Tanemura, S.; Toh, S.; Kaneko, K.; Nguyen, T. H.; Tanemura, M. *J. Ceram. Soc. Jpn.* **2004**, *112*, S1327–S1331.

(36) Miao, L.; Tanemura, S.; Toh, S.; Kaneko, K.; Tanemura, M. *Appl. Surf. Sci.* **2004**, *238*, 175–179.

(37) Wang, Y.; Zhang, L.; Deng, K.; Chen, X.; Zou, Z. *J. Phys. Chem. C* **2007**, *111*, 2709–2714.

(38) Sui, R.; Rizkalla, A. S.; Charpentier, P. A. *J. Phys. Chem. B* **2006**, *110*, 16212–16218.

(39) Sui, R.; Rizkalla, A. S.; Charpentier, P. A. *Langmuir* **2005**, *21*, 6150–6153.

(40) Cozzoli, P. D.; Kornowski, A.; Weller, H. *J. Am. Chem. Soc.* **2003**, *125*, 14539–14548.

(41) Wei, Q.; Hirota, K.; Tajima, K.; Hashimoto, K. *Chem. Mater.* **2006**, *18*, 5080–5087.

(42) Wu, Y.; Liu, H. M.; Xu, B. Q.; Zhang, Z. L.; Su, D. S. *Inorg. Chem.* **2007**, *46*, 5093–5099.

(43) Joo, J.; Kwon, S. G.; Yu, T.; Cho, M.; Lee, J.; Yoon, J.; Hyeon, T. *J. Phys. Chem. B* **2005**, *109*, 15297–15302.

(44) Trentler, T. J.; Denler, T. E.; Bertone, J. F.; Agrawal, A.; Colvin, V. L. *J. Am. Chem. Soc.* **1999**, *121*, 1613–1614.

(45) Schubert, U. *J. Mater. Chem.* **2005**, *15*, 3701–3715.

(46) Parra, R.; Goes, M. S.; Castro, M. S.; Longo, E.; Bueno, P. R.; Varela, J. A *Chem. Mater.* **2008**, *20*, 143–150.

(47) Sanchez, C.; Babonneau, F.; Doeuff, S.; Leaustic, A. *Ultrastructure Processing of Advanced Ceramics*; Wiley: New York, 1988.

(48) Sanchez, C.; Livage, J.; Henry, M.; Babonneau, F. *J. Non-Cryst. Solids* **1988**, *100*, 65–76.

Table 1. Structural and Physical Properties of As-Prepared and Calcined TiO$_2$ Xerogels at R = 3.5 and 5.5

			crystalline phase (wt fraction^b)		crystallite size^d (nm)		
sample	R (mol AcOH/mol Ti(O^{i}Pr)$_4$)	T^a (°C)	anatase	rutile	anatase	rutile	morphology
TiO$_2$-3.5$_{80C}$	3.5		^{c}	^{c}			spheres
TiO$_2$-3.5$_{400C}$	3.5	400	1.0	0.0	12.3		spheres
TiO$_2$-3.5$_{500C}$	3.5	500	0.99	0.01	16.3	^{e}	spheres
TiO$_2$-3.5$_{600C}$	3.5	600	0.49	0.51	29.4	34.5	spheres
TiO$_2$-5.5$_{80C}$	5.5		^{c}	^{c}			fibers
TiO$_2$-5.5$_{400C}$	5.5	400	1.0	0.0	13.0		fibers
TiO$_2$-5.5$_{500C}$	5.5	500	0.99	0.01	17.3	^{e}	fibers
TiO$_2$-5.5$_{600C}$	5.5	600	0.67	0.33	24.5	34.5	fibers
TiO$_2$-5.5$_{900C}$	5.5	900	0	1.0		64.0	fibers

[a] Calcination temperature. [b] Weight fraction of anatase (or rutile) calculated by a Zhang and Banfield correlation (sample calculations provided in the Supporting Information). [c] Amorphous product. [d] The diameter of the quasispherical crystallite determined by analysis of powder diffraction data (sample calculations provided in the Supporting Information). [e] Could not be determined because of insufficient concentration of rutile phase.

Transmission electron microscopy (TEM) images were obtained using a Philips Tecnai F20 operated at 200 kV. The samples were ground to a fine powder before being placed on a copper grid covered with holey carbon film. In situ IR studies were performed using a diamond immersion probe (ASI Applied Systems) attached to an ATR-FTIR spectrophotometer (ASI Applied Systems ReactIR 4000) that was managed by ReactIR 3.0 software (ASI). A chemometrics modeling program (SIMPLISMA) was carried out using the ACD UVIR Processor Version 8.0 software (ACD Inc., Toronto, Ontario). The offset α was set as a default at 20% during the SIMPLISMA modeling experiments; the input spectra were not smoothed or preprocessed. Electrospray mass spectra were recorded on isopropanol solutions directly infused to a Bruker Esquire 3000 mass spectrometer at a flow rate of 240 μL/h. Each spectrum was collected in the positive ion mode with the following parameters: skim 1 = 62.6 V, skim 2 = 6.0 V, and capillary exit = 151.8 V.

Results

Preparation of TiO$_2$ Nanostructures. The reaction of Ti(O^{i}Pr)$_4$ with AcOH in heptanes at T = 60 °C forms TiO$_2$ nanospheres or nanofibers at ambient pressures. The critical parameter dictating the morphology of the final product is the value of R: reactions carried out at lower acid ratios ($R \leq 3.8$) render nonuniform spherical nanoparticles; a network of monolithic TiO$_2$ nanofibers that are microns in length with diameters in the 10−20 nm range are formed at $R \geq 4.2$; and a mixture of fibers, spheres, and platelets are observed at the transition point of $R \approx 4.0$ (see Table S1 in the Supporting Information). Reactions carried out in hexanes yield similar results; however, lighter nonpolar solvents (e.g., pentanes) do not give rise to pure samples of fibers at R = 5.5. The reaction conditions described herein proceed in the same fashion at larger scales (i.e., up to at least 0.5 mol Ti(O^{i}Pr)$_4$). Given the breadth of possible synthetic conditions, only details of reactions carried out in heptanes at 11.0 mmol Ti(O^{i}Pr)$_4$ are provided in this study for the sake of brevity. Furthermore, the bulk of the results disseminated in this article focus on the fibrous products formed at $R \geq 4.2$ because the formation of spherical TiO$_2$ particles using the sol−gel process has been widely documented.[14,28,46]

The treatment of Ti(O^{i}Pr)$_4$ with AcOH results in the formation of a cloudy solution within 2−8 h. Continuous stirring ultimately produces a gel after ca. 7 h at R = 7.5; longer time periods are required at lower R values (e.g., 10 days at R = 3.5). Each gel was aged at 60 °C for an additional 5 days independent of gelation time to ensure that a monolithic xerogel is formed. The yield of each TiO$_2$ product was quantitative based on the Ti(O^{i}Pr)$_4$ precursor used in the reaction, thereby indicating the polycondensation reactions were driven to completion. Following aging, each of the samples were then heated to the respective calcination temperatures (e.g., 400, 500, or 600 °C) to form the respective xerogel (samples are denoted as TiO$_2$-R_{TC}, where T = temperature in °C; see Table 1).

Structural Characterization. SEM, TEM, and HRTEM images were collected to evaluate the structural morphology of the TiO$_2$ nanostructures. For samples synthesized over the R = 3.2−3.8 range, a random network of spherical particulates is prevalent, while randomly oriented nanofibers are observed for samples prepared over the R = 4.2−7.5 range (R = 5.5 is shown in Figure 1). The diameters of the fibers are relatively uniform with lengths on the micrometer scale and diameters over a relatively narrow size distribution of 10−20 nm. At 2000× magnification, the fibrous structures are smooth in appearance prior to calcinations (Figure 1a). The surface is degraded during thermal annealing, but the structures remain intact after heat treatment up to at least 900 °C. The HRTEM images of the fibers before calcination seem indicate a linear arrangement of macromolecules with diameters of 1.2 nm (Figure 1b, inset), whereas the calcined fibers are consistent with a chain of anatase nanocrystallites (Figure 1c, inset).

The powder X-ray diffraction (XRD) pattern of **TiO$_2$-5.5$_{400C}$** is consistent with a pure anatase crystalline phase (JCPDS Card No. 21-1272), which is also supported by the signature d-spacing of 3.5 Å of anatase (101) extracted from the HRTEM images. The progressive conversion to rutile occurs when the samples are heated to higher temperatures: samples heated at 500 °C for 2 h, **TiO$_2$-5.5$_{500C}$**, contain ca. 1% of the rutile phase (Figure S1), while calcination at 900 °C leads to the complete conversion of anatase to the rutile phase. The relative weight percentages of rutile and anatase in the samples, which were determined by a Zhang and Banfield correlation,[49] are listed in Table 1.

The size of the crystallites that comprise the xerogel were calculated using the signature anatase (101) and rutile (110) peaks in the XRD patterns according to Scherrer's equation.[50] Assuming spherical crystallites, the anatase structures within the fibers were found to be on the order of 13 and 24 nm at

---

(49) Zhang, H.; Banfield, J. F. *J. Phys. Chem. B* **2000**, *104*, 3481–3487.
(50) Weibel, A.; Bouchet, R.; Boulc'h, F.; Knauth, P. *Chem. Mater.* **2005**, *17*, 2378–2385.

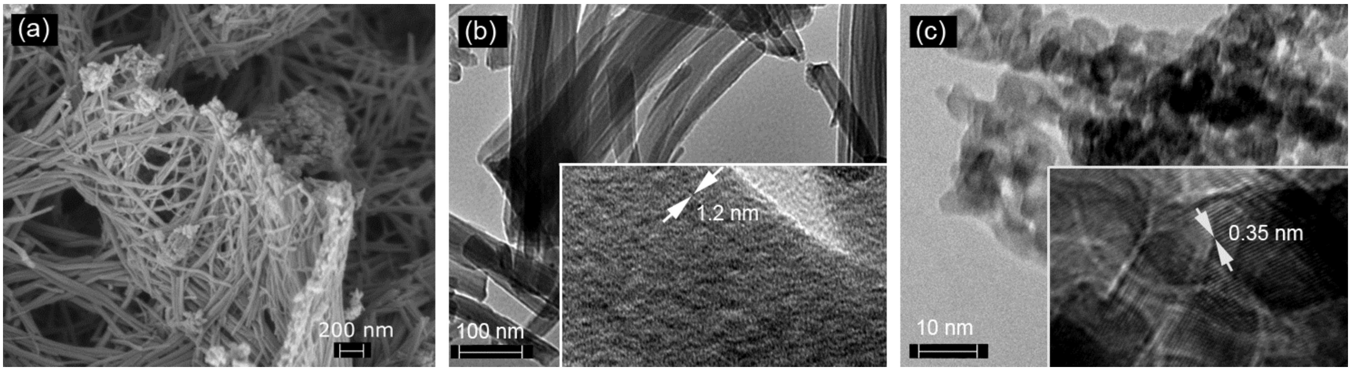

Figure 1. (a) SEM image of **TiO$_2$-5.5$_{400C}$**, and TEM and HRTEM (insets) images of (b) **TiO$_2$-5.5$_{80C}$** and (c) **TiO$_2$-5.5$_{400C}$**. A linear arrangement of macromolecules along the axis of the fiber corresponding to a diameter of ca. 1.2 nm is indicated in the HRTEM image of **TiO$_2$-5.5$_{80C}$**. The HRTEM image of **TiO$_2$-5.5$_{400C}$** highlights the *d*-spacing of 0.35 nm for the (101) plane of anatase within the fibrous bundles.

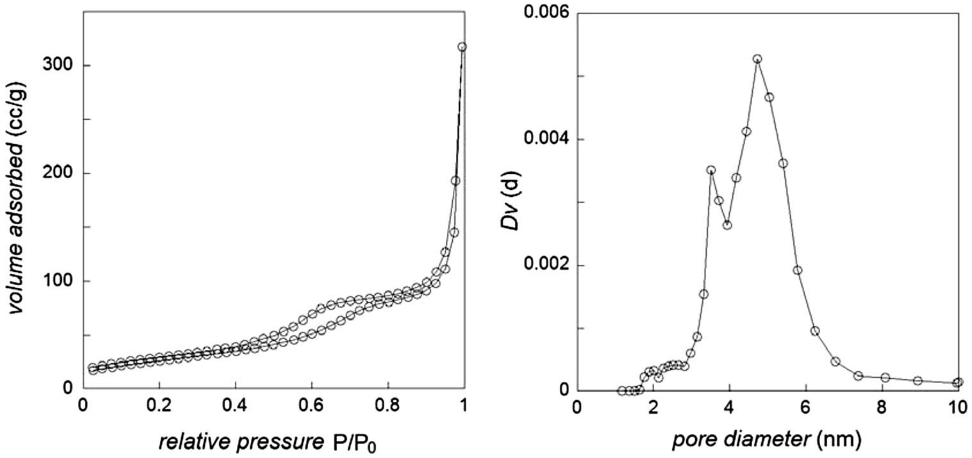

Figure 2. (a) N_2 physisorption isotherms and (b) BJH pore-size distributions of **TiO$_2$-5.5$_{400C}$**. (Dv = derivative of volume adsorbed.)

400 and 600 °C, respectively. Similarly, the rutile crystallites were ca. 34 and 64 nm for the xerogels calcined at **TiO$_2$-5.5$_{600C}$** and **TiO$_2$-5.5$_{900C}$**, respectively (Table 1). These trends indicate that the size of the respective anatase and rutile crystallites within the fibers increase upon heating suggesting that crystallites fuse together at higher calcination temperatures. This trend is also observed for the spherical particles (Table S1).

N_2 Physisorption Measurements. The specific Brunauer–Emmett–Teller (BET)[51,52] surface areas of the fibrous TiO_2 xerogels produced at $R = 5.5$ were found to be 223 and 95 m^2/g before and after calcination at 400 °C, respectively. The calcined samples (**TiO$_2$-5.5$_{400C}$**) exhibit type IV isotherms consistent with a mesoporous framework (Figure 2),[52] and H3 hysteresis loops indicative of slitlike pores between the nanofibers within the bundles. The Barret–Joyner–Halenda (BJH) desorption analysis[52,53] indicates a bimodal pore size distribution for the nanofibers with maxima at diameters of 3.5 and 4.7 nm (Figure 2).

Electronic and Vibrational Spectroscopy. UV-vis absorbance spectra were recorded on various TiO_2 xerogels to measure the effect of calcination temperature on the band gap (E_g). The E_g for **TiO$_2$-5.5$_{80C}$** is 3.24 eV (382 nm) based on the absorption edge of the absorbance spectra, and is shown to diminish slightly with increasing calcination temperature from 3.14 eV (393 nm) at 400 °C to 2.92 eV (423 nm) at 900 °C (Figure S2). This trend confirms the onset of a phase transition from anatase to rutile at higher calcination temperatures (E_g of anatase and rutile are 3.2 and 3.0 eV, respectively[54,55]), which is consistent with the attendant powder X-ray diffraction data.

FTIR difference spectra were recorded to extract structural information of the fibrous structures before and after calcination; spectra for fibers prepared at $R = 5.5$ are shown in Figure 3 together with relevant starting materials. The signals at ca. 2980 cm^{-1} are assigned to the C–H stretching modes of ligated $^{-}$OAc and residual ^{i}PrOH. The carbonyl stretches associated with free carboxylic acid and H-bonded acid groups appear at ~1750 cm^{-1} and 1701–1730 cm^{-1}, respectively.[56] Lower intensity signals at 1347 and 1028 cm^{-1} are assigned to the C–C stretching modes of acetate bound to Ti;[56] the signal at 1242 cm^{-1} to the C–O stretching mode emanating from Pr^{i}OAc. The low energy signals at

---

(51) Brunauer, S.; Emmett, P. H.; Teller, E. *J. Am. Chem. Soc.* **1938**, *60*, 309–19.

(52) Sing, K. S. W.; Everett, D. H.; Hal, R. A. W.; Moscou, L.; Pierotti, R. A.; Rouquerol, J.; Siemieniewska, T. *Pure Appl. Chem.* **1985**, *57*, 603–619.

(53) Barrett, E. P.; Joyner, L. G.; Halenda, P. P. *J. Am. Chem. Soc.* **1951**, *73*, 373–80.

(54) Li, J. G.; Ishigaki, T.; Sun, X. *J. Phys. Chem. C* **2007**, *111*, 4969–4976.

(55) Hoffmann, M. R.; Martin, S. T.; Choi, W.; Bahnemann, D. W. *Chem. Rev.* **1995**, *95*, 69–96.

(56) Liao, L.-F.; Lien, C.-F.; Lin, J.-L. *Phys. Chem. Chem. Phys.* **2001**, *3*, 3831–3837.

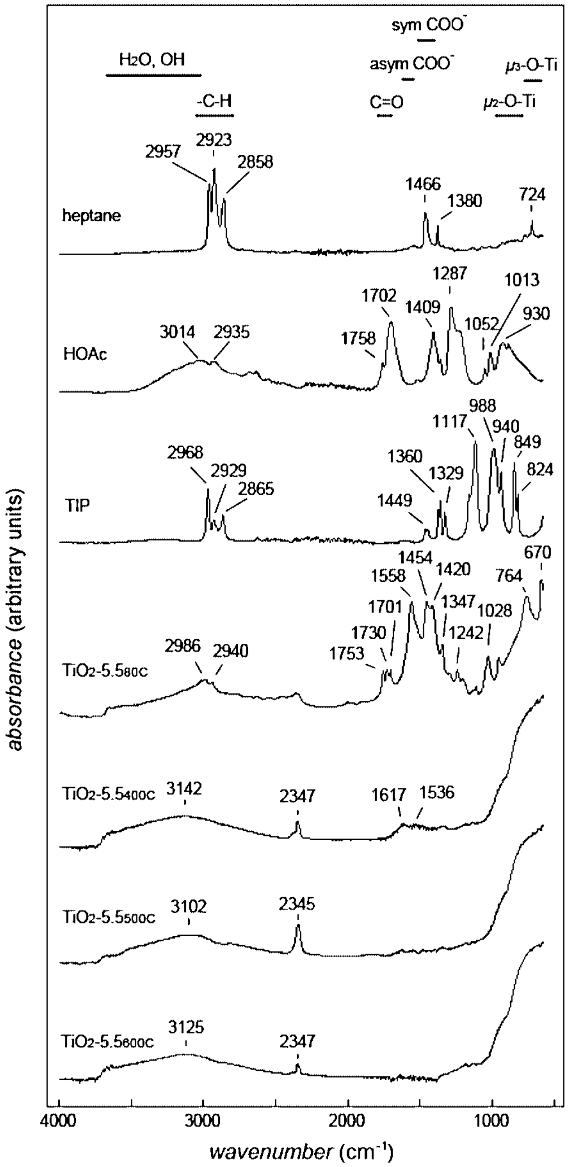

Figure 3. FTIR spectra of nanofibrous TiO_2 xerogels before (**TiO_2-5.5$_{80C}$**) and after calcination (**TiO_2-5.5$_{400C}$**, **TiO_2-5.5$_{500C}$**, and **TiO_2-5.5$_{600C}$**). Spectra for the reagents (AcOH, $Ti(O^iPr)_4$) and solvent (heptanes) used for xerogel preparation are provided for reference purpose. (The signal at ~2345 cm^{-1} is attributed to CO_2.)

764 and 670 cm^{-1} correspond to μ_2- and μ_3-oxide bridging motifs, respectively.[57]

The nature of the unprotonated carboxylato binding modes present within these systems is typically characterized by the symmetric stretching modes (ν_{sym}) at 1454 and 1420 cm^{-1}, and the asymmetric mode (ν_{asym}) at 1558 cm^{-1} (Scheme 1).[38,58−62] The small difference in these two modes (~100 cm^{-1}) rules out the presence of a unidentate ester linkage, which would be expected to give rise to a much larger separation.[63] The lower observed splitting suggests that the carboxylato groups use both O atoms to bind to one (chelating bidentate) or two (bridging bidentate) Ti atoms (Scheme 1). Because a separation of less than 100 cm^{-1} and a ν_{asym} signal at <1540 cm^{-1} are signature features of the former, we assign the signal observed at 1558 cm^{-1} to the bridging bidentate mode. This assignment is endorsed by previous studies that state that the bidentate chelating ν_{asym} modes reside at energies higher than 1540 cm^{-1}.[58,60,61] The absence of organic C−H, C−C, and C−O stretching modes in the spectra of the calcined samples indicates the $AcOv^-$ and $^iPrOv^-$ groups are removed upon heating. The concomitant formation of TiO_2 is confirmed by the Ti−O bonding modes observed below 900 cm^{-1}. Similar powder IR spectra for the spherical particles were also observed and provided in Figure S4 of the Supporting Information.

Scheme 1. Possible Ti-OAc Binding Modes

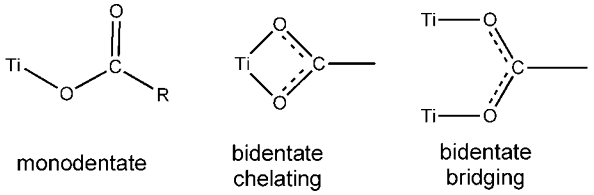

In situ FTIR Studies. In situ ATR-FTIR spectroscopy was used to track the course of the polycondensation reactions following the addition of $Ti(O^iPr)_4$ to AcOH. Experiments were carried out at 60 °C using 33 mmol of $Ti(O^iPr)_4$ in 12 mL of heptanes with variable quantities of AcOH ($R = 3.5$, 5.5 and 7.5) injected into the reaction chamber to reflect the synthetic conditions described in the experimental section. The reaction solution was vigorously stirred immediately following the addition of AcOH, and the first spectrum was recorded 0.5 min after the reagents were combined; data was collected every 0.5 min for 10 min, and then every 10 min for 770 min. Spectra recorded on the mixture at $R = 5.5$ are provided in Figure 4a. Reaction kinetics were elucidated by assessing the bridging bidentate Ti-OAc signals over the 1400−1650 cm^{-1} range (Figure 4b) over a 13 h time frame. This region was selected because it effectively avoids spectral overlap with other species present in solution; e.g., monitoring the disappearance of $Ti(O^iPr)_4$ in the 820−1360 cm^{-1} range could not be carried out due to the superposition of signals corresponding to acetate, alcohols, and esters.

The reaction of $Ti(O^iPr)_4$ with AcOH in heptanes produces a significant number of intermediates in solution; however, we are able to track the reaction as it proceeds through two major reaction phases: (i) hydrolysis of the hexanuclear titanium-acetate complex (TAC), $TiO_6(OAc)_6(O^iPr)_6$ (**TAC1**), to form substitution intermediates formulated as $Ti_6O_6(OAc)_6(O^iPr)_{6-n}(OH)_n$ ($0 < n \leq 6$; **TAC2**); and (ii) intermolecular condensation of the **TAC2** clusters to form the linear macromolecules that lead to the final products, **TiO_2-R_{60C}**. The relative rates of these two key reaction phases were monitored by monitoring the respective formation and consumption of these three principle species.

---

(57) Qu, Z. w.; Kroes, G. J *J. Phys. Chem. B* **2006**, *110*, 8998–9007.

(58) Barrow, H.; Brown, D. A.; Alcock, N. W.; Clase, H. J.; Wallbridge, M. G. H. *J. Chem. Soc., Dalton Trans.* **1994**, 195–199.

(59) Kils, K.; Mayo, E. I.; Brunschwig, B. S.; Gray, H. B.; Lewis, N. S.; Winkler, J. R. *J. Phys. Chem. B* **2004**, *108*, 15640–15651.

(60) Boyle, T. J.; Tyner, R. P.; Alam, T. M.; Scott, B. L.; Ziller, J. W.; Potter, B. G. *J. Am. Chem. Soc.* **1999**, *121*, 12104–12112.

(61) Doeuff, S.; Dromzee, Y.; Taulelle, F.; Sanchez, C. *Inorg. Chem.* **1989**, *28*, 4439–4445.

(62) Rammal, A.; Brisach, F.; Henry, M. *C. R. Chim.* **2002**, *5*, 59–66.

(63) Nakamoto, K. *Infrared and Raman Spectra of Inorganic and Coordination Compounds*; Wiley: New York, 1997.

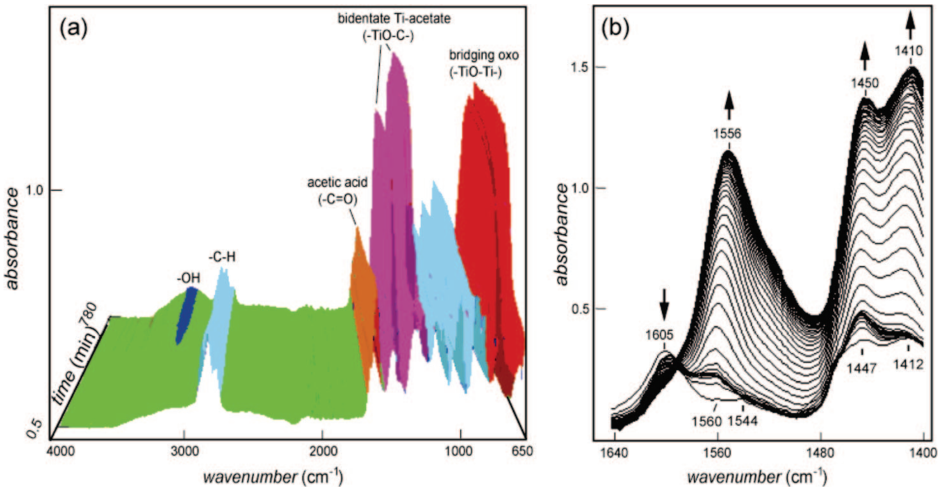

Figure 4. (a) In situ FTIR spectra for **TiO_2-5.5$_{60C}$** over a 13 h time period (11 mmol $Ti(O^iPr)_4$; $R = 5.5$; $T = 60$ °C). The first spectrum was recorded 0.5 min after injection of AcOH into the reaction chamber containing $Ti(O^iPr)_4$ in heptanes. (b) Expanded region highlighting the signature ν_{COO-} signals (1400−1640 cm^{-1}) as a function of time. (Arrows indicate progressive trends of data with time.)

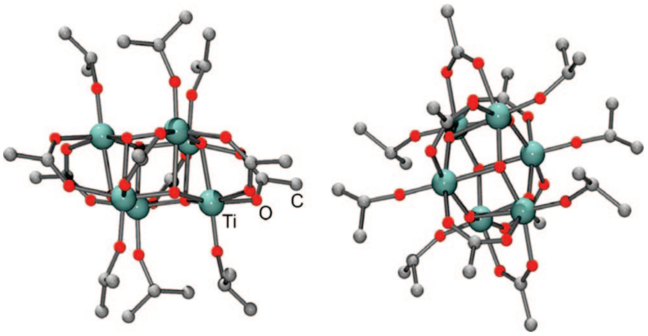

Figure 5. Molecular structure of $Ti_6O_6(OAc)_6(O^iPr)_6$ (**TAC1**) viewed along the *a* (left) and *c* (right) axes. (Ti = aquamarine; O = red; C = gray; H atoms omitted for clarity.) (This structure was previously reported by Charpientier[64] and is provided only to highlight the axial and equatorial coordination of the $^iPrO^-$ and AcO^- ligands, respectively.[64])

The premise of this analysis relies on accurately defining the spectral profiles of **TAC1**, **TAC2**, and **TiO_2-*R*$_{60C}$**. Fortunately, the spectrum of the reaction mixture 0.5 min after mixing $Ti(O^iPr)_4$ with AcOH is congruent with the spectral profile of **TAC1** reported elsewhere.[38,64] Using single-crystal X-ray diffraction methods, these studies demonstrated that **TAC1** corresponds to the hexanuclear framework depicted in Figure 5. We confirmed that **TAC1** forms in less than 1 min by electrospray ionization mass spectrometry (ESI-MS) experiments (vide infra); thus, we are confident in assigning the in situ spectrum at $t = 0.5$ min to **TAC1**. With the FTIR spectrum of the final condensation product, **TiO_2-*R*$_{60C}$**, also established (Figure 3), the in situ data could be separated into three principle components, where the third constituent corresponds to **TAC2**. We caution that we are unable to confirm whether **TAC2** is a single molecular entity (e.g., $Ti_6O_6(OAc)_6(OH)_6$), or a mixture of substitution products that results from the stepwise hydrolysis of $^iPrO^-$ groups ligated to the Ti centers. We therefore assign **TAC2** as one or a mixture of products encompassed by the formula, $Ti_6O_6(OAc)_6(O^iPr)_{6-n}(OH)_n$ (where $6 \geq n < 0$). The spectra corresponding to these three components could therefore be deconvoluted using SIMPLISMA software[65,66] at each value of *R* to generate respective time-dependent concentration profiles (Figure 6 and Table S2).

Inspection of the spectral profiles at $R = 3.5$ show that the concentration of **TAC1** exhibits a rapid decrease down to 80% of the original concentration within $t = 6$ min, then gradually decreases down to 330 min, followed by an accelerated decrease in concentration until the consumption of **TAC1** is complete at 550 min (Figure 6a). The decreasing concentration of **TAC1** is concomitant with the increasing concentration profiles of both **TAC2** and **TiO_2-3.5$_{60C}$** until 330 min, at which point **TAC2** is consumed faster than it is generated until it is exhausted entirely at 800 min.

Data recorded at progressively higher acid ratios (Figure 6b and 6c) reveal that the relative concentration of AcOH to $Ti(O^iPr)_4$ plays a fundamental role in the kinetics of the reaction. At higher values of *R*, the concentration profiles of **TAC1, TAC2** and **TiO_2-5.5$_{60C}$** are similar to those recorded at $R = 3.5$, except each process occurs at a relatively faster rate. For instance, the transition corresponding to the sudden decrease in the concentration of **TAC2** occurs at 180 min instead of 330 min, while at $R = 7.5$ this same transition occurs at 80 min. Likewise, **TAC1** is completely consumed in 210 min at $R = 7.5$, but not until 300 and 550 min at $R = 5.5$ and 3.5, respectively. A full interpretion of these results is provided in the Discussion.

Electrospray Ionization Mass Spectrometry Studies. In order to confirm that the precursor, **TAC1**, is formed rapidly in solution, the species generated during the early stage of the reaction was probed using ESI-MS techniques. Immediately following the combination of $Ti(O^iPr)_4$ with HOAc in hexanes, the reaction solution was directly injected into the mass spectrometer; the mass spectrum recorded within 1 min is provided in Figure 7; the corresponding assignments are listed in Table S3 of the Supporting Information. These data reveal the rapid formation of numerous molecular fragments ranging in metal content from 2 to 6 Ti centers.

---

(64) Sui, R.; Charpentier, P. A.; Rizkalla, A. S.; Jennings, M. C. *Acta Crystallogr., Sect. E* **2006**, *62*, m373–m375.

(65) Windig, W.; Antalek, B.; Lippert, J. L.; Batonneau, Y.; Bremard, C. *Anal. Chem.* **2002**, *74*, 1371–1379.

(66) Windig, W.; Stephenson, D. A. *Anal. Chem.* **1992**, *64*, 2735–2742.

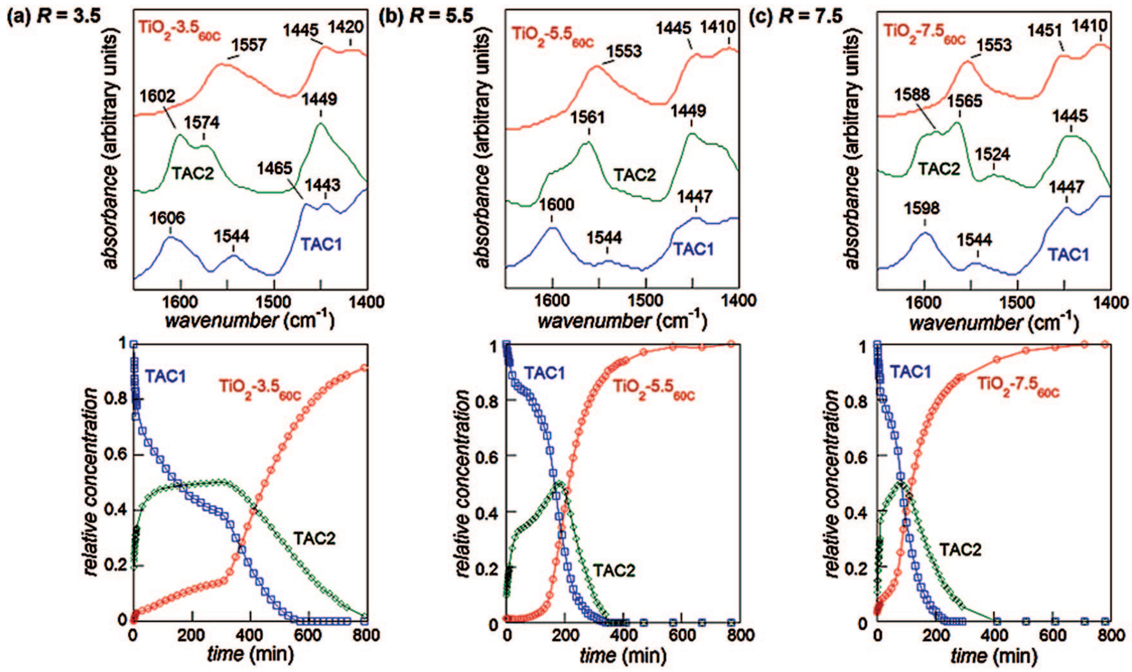

Figure 6. Calculated spectra (top) and the corresponding time-dependent concentration profiles (bottom) of titanium−acetate complexes (**TAC1**, **TAC2**) and condensation products at variable values of *R* (**TiO_2-3.5$_{80C}$**, **TiO_2-5.5$_{80C}$**, and **TiO_2-7.5$_{80C}$**).

Unfortunately, the precise number of AcO^- and O^iPr^- ligands in the cluster could not be resolved because the molecular weights of both compounds are 59.0 g/mol. Nonetheless, these results reveal no evidence of $Ti(O^iPr)_4$ 0.5 min after the reaction is initiated, and the signals centered at *m*/*z* 1032 amu indicate that a hexanuclear cluster is formed. The majority of the signals at lower *m*/*z* values are assigned as daughter peaks of the principle mass fragment at *m*/*z* 1032 amu based on MS/MS studies. We note that this does not rule out the presence of lower nuclearity clusters in solution, but the congruence of the in situ FTIR data to the spectrum of single crystals of **TAC1** provides strong evidence that the hexanuclear cluster is the major species in solution at 0.5 min.

Discussion

We have found that mixing $Ti(O^iPr)_4$ with AcOH in heptanes at $T = 60$ °C forms TiO_2 nanospheres or nanofibers at moderate temperatures. The morphology of the final product is inherently sensitive to the value of *R*: reactions carried out at lower *R* (≤3.9) render agglomerated spherical nanoparticles, while one-dimensional structures are formed when $R \geq 4.2$.

On the basis of the in situ ATR-FTIR, the value of *R* appears to directly affect the rate of hydrolysis of the titanium-acetate complexes that form in solution during the early stage of the reaction. Acetic acid is critical during this reaction phase because it serves to generate ^iPrOH upon modification of $Ti(O^iPr)_4$ (R1), which, in turn, triggers the formation of H_2O upon esterification with AcOH (R2). The rate of R2 is inherently slow in the absence of a catalyst, but is accelerated when $Ti(O^iPr)_4$ is present (the coordinatively unsaturated Ti complex acts as a Lewis acid catalyst by enhancing the electrophilicity of the carboxylate). Because the reactions are carried out in pure organic solvents, the subsequent hydrolysis and condensation steps with the metal species are dictated by the rate and quantity of water released during this esterification process. A consequence of this process is that higher quantities of AcOH lead to higher concentrations of ^iPrOH, which then enhances the rate of esterification.

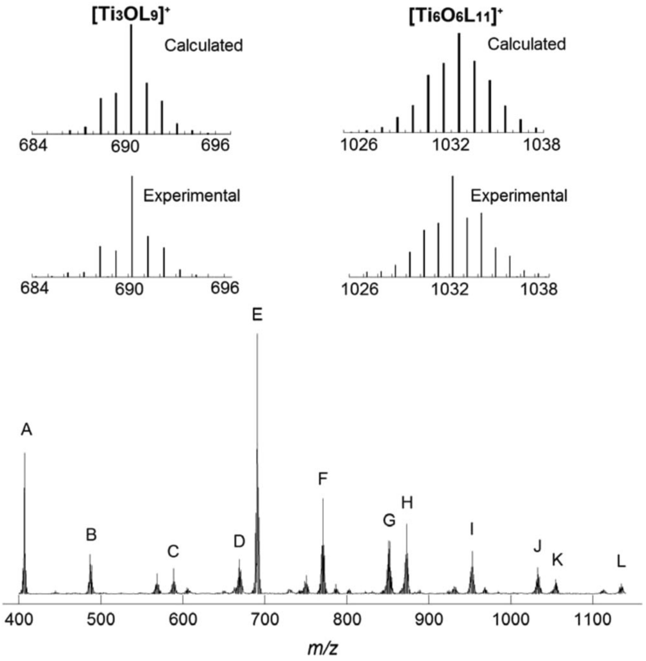

Figure 7. Electrospray positive-ion experimental and calculated mass spectra of $Ti(O^iPr)_4$ in heptanes 0.5 min after combination with 5.5 mol equiv of AcOH. Selected *m*/*z* signals in the parent ion region are indicated; *m*/*z* signal assignments are listed in Table S3 (L = AcO^- and $^iPrO^-$).

The liberated water provides access to a number of hydrolysis and condensation processes to ultimately form the hexanuclear intermediate **TAC1**. Despite the numerous possible intermediates that can arise from these reactions,[67–69] it has been shown by others[38,64,70] that similar reaction conditions ultimately converge on this hexanuclear species. We have confirmed this pathway by way of mass spectrometry, which show the formation of a molecular species consistent with **TAC1** within 0.5 min. (We emphasize that ESI-MS is a powerful tool for extracting structural information of titanium-oxide intermediates, but has little precedent in the literature.[71]) Although this mass spectrum contains a number of smaller molecular fragements, many of these are due to the fragmentation of the higher nuclearity clusters during the course of the measurements. This was confirmed not only by MS/MS data, but also the correlation of the spectrum to that of a solution containing dissolved crystals of **TAC1** (Supporting Information). The net reaction describing the formation of **TAC1** is expressed by R3. The hydrolysis of the hexanuclear building block, **TAC1**, leads to one of the intermediates denoted as **TAC2** (R4), which then undergoes subsequent condensation reactions that lead to the formation of the final product (R5). The condensation of the **TAC2** clusters into macromolecules leads to the release of additional water molecules that also help drive the reaction to completion.

$$Ti(O^iPr)_4 + n\mathrm{AcOH} \rightleftharpoons Ti(O^iPr)_{4-n}(OAc)_n + n\,{}^iPrOH \qquad (R1)$$

$$AcOH + {}^iPrOH \rightleftharpoons {}^iPrOAc + H_2O \qquad (R2)$$

$$6Ti(O^iPr)_4 + 18AcOH \rightleftharpoons Ti_6O_6(OAc)_6(O^iPr)_6\ (\mathbf{TAC1}) + 6\,{}^iPrOH + 12\,{}^iPrOAc + 6H_2O \qquad (R3)$$

$$Ti_6O_6(OAc)_6(O^iPr)_6\ (\mathbf{TAC1}) + nH_2O \rightleftharpoons Ti_6O_6(OAc)_6(O^iPr)_6(OH)_n\ (\mathbf{TAC2}) + n\,{}^iPrOH \qquad (R4)$$

$$m Ti_6O_6(OAc)_6(OH)_6\ (\mathbf{TAC2}) \rightleftharpoons [Ti_6O_9(OAc)_6]_m + 3mH_2O \qquad (R5)$$

We contend that the morphology of the final product is directly related to the extent **TAC2** is hydrolyzed. If R is sufficiently high, we anticipate that the axial ${}^iPrO^-$ ligands of **TAC1** to be fully displaced by OH^- groups (i.e., $n = 6$ in R4). The subsequent condensation of these clusters can then occur at all three axial sites on each face of the cluster, a scenario that would facilitate the growth of 1D macromolecules (Scheme 2). If the hydrolysis of the axial ${}^iPrO^-$ ligands of **TAC1** is incomplete where **TAC2** represents a species that contains a mixture of axial ${}^iPrO^-$ and OH^- ligands (e.g., $0 < n < 6$ in R4), then the axial condensation of macromolecules is impeded and spherical particles are formed (Scheme 2).

Scheme 2. Proposed Formation of Fibrous and Spherical Particulates As a Function of R^a

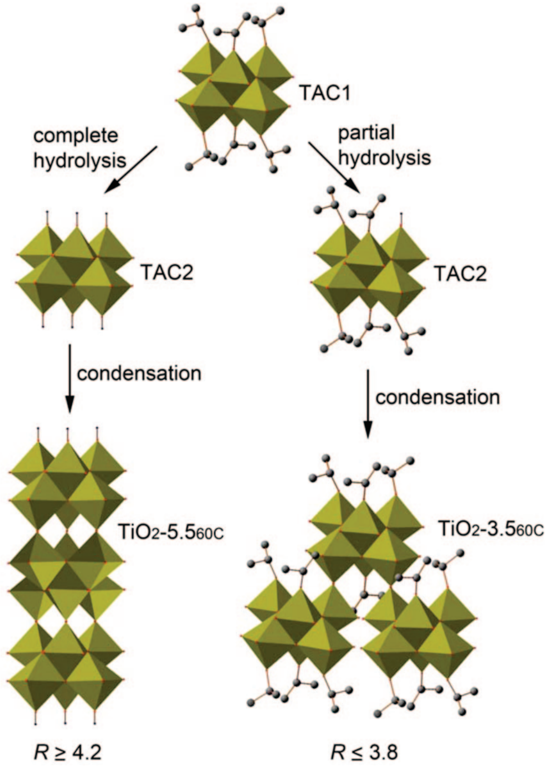

[a] Octahedral TiO_6 units = green octahedrons; O = red; C = grey; hydroxide H atoms = black; all other H atoms and acetate ligands omitted for clarity.

On this basis, the topology of the final product should be dictated largely by the amount of water that is generated in situ, which is affected by the amount of AcOH present in solution. This is qualified by evaluating the above reactions that actually generate water over the course of the reaction; namely, R2, R3, and R5. The liberation of water during the esterification step (R2) demands that sufficient quantities of AcOH be present in solution. A high concentration of AcOH will shift the equilibria for both R1 and R2 toward the respective products, with the esterification step (R2) representing the rate-limiting step. Because this esterification reaction is catalyzed by $Ti(O^iPr)_4$, water is generated quickly during the initial stages to quickly form **TAC1** until $Ti(O^iPr)_4$ has been exhausted. This is reflected by the rapid decrease of the **TAC1** concentration profile (at $t < 6$ min) in Figure 6. We note that similar data is obtained in strictly anhydrous conditions, thereby ruling out trace water impurities being responsible for this behavior. The condensation of Ti fragments to form **TAC1** also produce water, but this can only occur after an equal quantity of water is consumed in R3; thus, these steps are expected to have a minimal net effect on the H_2O content present in solution. The condensation of the macromolecules in R4, however, liberates a significant quantity of water (up to 3 H_2O molecules per **TAC2**) that can then serve to accelerate the formation of the macromolecules in the latter stages of the reaction. This autocatalytic process appears to propel the condensation reaction (e.g., at $t > 330$ min for $R = 3.5$) to ultimately drive the reaction to completion. Collectively, these results highlight the delicate balance for the formation of nanofibers: the liberation of water needs to be controlled to avoid rapid precipitation, while a sufficient quantity of water needs to

---

(67) Birnie, D. P.; Bendzko, N. J. *Mater. Chem. Phys.* **1999**, *59*, 26–35.
(68) Doeuff, S.; Dromzee, Y.; Sanchez, C. *C. R. Acad. Sci., Ser. 2* **1989**, *308*, 1409–12.
(69) Laaziz, P. I.; Larbot, A.; Guizard, C.; Durand, J.; Cot, L.; Joffre, J. *Acta Crystallogr, Sect C* **1990**, *46*, 2332–4.
(70) Papiernik, R.; Hubert-Pfalzgraf, L. G.; Vaissermann, J.; Goncalves, M. C. H. B. *J. Chem. Soc., Dalton Trans.* **1998**, 2285–2288.
(71) Khitrov, G. A.; Strouse, G. F.; Gaumet, J.-J. *J. Am. Soc. Mass Spectrom.* **2004**, *15*, 260–267.

be generated to drive the complete hydrolysis of the axial isopropoxide ligands to facilitate axial condensation of the macromolecules.

The condensation of the fully hydrolyzed hexanuclear **TAC1** structures to form a linear collection of macromolecules is supported by HRTEM studies (Figure 1b, inset), which reveal a linear chain of macromolecules characterized by diameters of ca. 1.2 nm. This value resonates with the diameter of 1.1 nm for the hexanuclear cluster, $Ti_6O_6(OAc)_6(O^iPr)_6$ (**TAC1**) (defined by the distance spanning the terminal C atoms from distal AcO^- ligands on a single cluster). The signal at *m*/*z* 1032 amu in the mass spectrum of the reaction mixture after 0.5 min, along with the in situ IR data, further corroborates the existence of the hexamer, $Ti_6O_6(OAc)_6(O^iPr)_6$ (**TAC1**),[38] as an intermediate building block within the TiO_2 fibrous structure.

The as-prepared samples indicated a smooth surface, but after calcination, the fibers are shown to be a collection of nanocrystallites. While this feature may hinder the role of these materials in applications where high electrical continuity is desired, the high surface areas retained by the fibers may provide utility in select photocatalytic schemes (note that the BET surface area of the calcined fibers (95 m^2/g at $R = 5.5$) are approximately 2-fold higher than that of commercial Degussa P25 TiO_2 nanoparticles[72]).

Conclusions

High-aspect-ratio TiO_2 nanofibers can be prepared at low temperatures and ambient pressure in nonpolar organic solvents. This preparation method, which avoids the use of exotic precursors, highlights the role that stoichiometry has on the shape of the final product. A kinetic analysis shows that the formation of the macromolecules is slow during the initial phase of the reaction, and is accelerated when the condensation of the TACs formed in situ liberate water more efficiently at higher relative concentrations of AcOH. Our efforts are currently focused on exploiting this method to gain greater control of the aspect ratio of these TiO_2 materials, and to incorporate dopants (e.g., Sn, N) to further influence the electronic structure of these materials.

Acknowledgment. We thank Richard Humphrey of Micro-Science Enterprises Ltd. and Dr. Todd Simpson of the Nanomanufacture Laboratory at the University of Western Ontario. From the University of Calgary, we thank Dr. Warren Piers, Dr. Todd Sutherland, Dr. Thomas Baumgartner, Rapheal Jiminez, Yi Ren, Jason Young, Shihua Zhang, W. Michael Schoel, Wei Dong, and Blessing Ibeh for access to and assistance with instrumentation. This work was financially supported by Canada Research Chairs, a Discovery Grant from the Natural Science and Engineering Research Council of Canada, an Alberta Ingenuity New Faculty Award, and the Institute for Sustainable Energy, Environment & Economy.

Supporting Information Available: . Listing of TiO_2 morphologies for samples prepared over the $R = 2.5-7.5$ range, the calculated acetate ν_{COO^-} modes corresponding to the three principal species, sample calculations for selected data in Table 1, powder XRD for **TiO_2-5.5**, UV-vis spectra for **TiO_2-3.5** and **TiO_2-5.5**, FTIR spectra for **TiO_2-3.5**, and ESI-MS spectra for **TAC1** (PDF). This material is available free of charge via the Internet at http://pubs.acs.org.

CM802091C

---

[72] Asilturk, M.; Sayilkan, F.; Erdemoglu, S.; Akarsu, M.; Sayilkan, H.; Erdemoglu, M.; Arpac, E. *J. Hazard. Mater.* **2006**, *129*, 164–170.